Optimal Allocation of Energy Storage System in DFIG Wind Farms for Frequency Support Considering Wake Effect

Linyun Xiong, Shaobo Yang, Sunhua Huang, Donglin He, Penghan Li, Muhammad Waseem Khan, and Jie Wang

***Abstract*—Energy storage systems (ESSs) are being utilized to improve wind farms' (WF) frequency support capability due to their high reliability, fast response and the dual role of energy users and suppliers. Nevertheless, the problem of how much capacity should each ESS possesses in order to better serve the WFs has never been investigated. With this perspective, this paper proposes an optimal ESS allocation (OEA) scheme for doubly fed induction generator (DFIG) based WFs to mitigate the impact of wake effect in frequency support. Firstly, the synchronous stability of wind turbines under frequency dips is analyzed with the concept of frequency support margin (FSM), and the detrimental impact of the wake effect is also investigated. Subsequently, the role of ESSs to improve wind turbines' synchronous stability is demonstrated. To make the OEA scheme practical, the wind turbines in a WF are segmented into different clusters based on the received wind speed. Afterwards, the OEA problem is formulated, where the objective is to optimize the coherency of the wind turbine clusters' FSM level. The simulation results show that ESS can provide secondary frequency support under major grid frequency drops, and the proposed OEA scheme can reduce the risk of loss of synchronous stability.**

***Index Terms*—Energy storage system (ESS), doubly fed induction generator (DFIG), frequency support, wake effect, synchronous stability.**

I. Introduction

THE increasing penetration of wind power into the main power grid has brought about critical challenges for the system security, especially the frequency security of the system. As the system frequency stability can be maintained on basis of the active power balance between the supply and the load side, power grids with high share of wind energy cannot effectively guarantee the sufficient output of power to meet the demand, forcing the system to lower down the frequency and leading to frequency stability issues [1]. Thus, wind farms (WFs) should be capable of providing frequency support for the main power grid, especially when the power grid is highly penetrated with wind power.

Due to the decoupling of wind turbine (WT) rotor speed with the grid frequency, the WTs will not naturally respond to frequency deviations. Instead, extra control strategies have to be applied to improve WT's inertial response capability, including virtual inertia control, rotor speed control, pitch angle control, and frequency droop control [2]–[4]. As wind energy plays a more vital role in system operation, its importance in power system primary frequency response and inertial response is being validated by more industrial applications and academic researches [5]. In [6], the impact of wind power generation on the grid is evaluated on the U.S. Western Interconnection. It is proven that inertial and primary frequency response control from WFs can improve the system frequency response under different penetration level. In [7], the operation limit for DFIGs to provide frequency control in a steady manner is analyzed, where the controller tuning tactics are developed to prevent the turbines to stall due to over draining of the kinetic energy. Apart from the aforementioned simulation based researches, there are a few field trial based research reports. In 2019, Australian wind turbine equipment manufacturer Goldwind conducted a series of field trials at the Gullen Range Wind Farm to test the WF's capability of providing frequency support. Utilizing the inertia based fast frequency response approach, 10 WTs are tested and they consistently achieved frequency response of up to 10% of nameplate capacity, 6 seconds of boost duration, a ramp delay of less than 2 seconds and a time to peak less than 2 seconds [8]. In [9], a series of real field implementation and trial experiments are reported to test the power production capability of two 2MW turbines from the Le Sole de Moulin Vieux WF when the wind turbine aerodynamic interactions are considered. Several experimental tests are conducted at a 70MW WF in Canada to compare the performance of WFs' control loops in the field trials and simulation scenarios, including the WFs' ability to respond to grid frequency [10]. Other than that, the concept of virtual synchronous generators is implemented in Zhangbei WF, where the rotor inertial control is tested via field experiments on a 2MW WT [11]. In this field trial research, the WT can yield

Manuscript received March 1, 2021; revised June 1, 2021 and July 13, 2021; accepted September 2, 2021. Date of publication September 13, 2021; date of current version April 19, 2022. This work was supported in part by the National Natural Science Foundation of China under Grant 52007015, in part by the Natural Science Foundation of Chongqing, and in part by the Natural Science Foundation Key Project of Chongqing under Grant cstc2019jcyj-zdxmX0005 Paper no. TPWRS-00331-2021. *(Corresponding authors: Linyun Xiong; Sunhua Huang.)*

Linyun Xiong, Shaobo Yang, and Donglin He are with the School of Electrical Engineering, Chongqing University, Chongqing 400044, China (e-mail: 1669554200@qq.com; shaoboyang@cqu.edu.cn; donglinhe@cqu.edu.cn).

Sunhua Huang, Penghan Li, Muhammad Waseem Khan, and Jie Wang are with the School of Electronic Information and Electrical Engineering, Shanghai Jiao Tong University, Shanghai 200240, China (e-mail: sunhuahuang@sjtu.edu.cn; penghanli@sjtu.edu.cn; muhammadkhan@sjtu.edu.cn; jiewang@sjtu.edu.cn).

Color versions of one or more figures in this article are available at https://doi.org/10.1109/TPWRS.2021.3111017.

Digital Object Identifier 10.1109/TPWRS.2021.3111017

supplementary power of 48.7% of the rated capacity after the grid frequency declines, lasting for 20.7s until the rotor speed reaches the lower limit. It needs to note that all the field trials utilize analogy to realize the grid frequency drops in the control block, as it is impossible to trigger a real grid frequency drop in the experiment. Nevertheless, these field trials and experiments fully validated the potential and necessity of WTs to contribute to the grid frequency regulation.

To equip the WTs with the capability of providing fast and reliable frequency services, several novel approaches are being implemented. In [12], a safety supervisory control is developed to synthesize the frequency support modes of WTs such that adequate frequency response abilities of the WFs can be ensured. Nevertheless, the provision of frequency support via WT may result in secondary frequency dips due to the need for rotor speed recovery. Thus, a dynamic demand control strategy is proposed to coordinate with the DFIG WT's control such that adequate inertial response can be ensured with secured rotor speed [13]. With the penetration of renewable energy sources (RESs) like WT, the power system will gradually lose its original inertia due to the replacement of the synchronous generators with RESs and it will become a low inertia system. Thus, several recent researches are dedicated to enhancing the frequency response ability and system security of WTs which are integrated in low-inertia systems. For example, in [14], a novel frequency control strategy which incorporates AC voltage control is proposed to enable the offshore WTs to provide frequency support for low-inertia onshore grid via a HVDC transmission network; in [15], a resonance damper is proposed to mitigate the possible resonance between WTs and the low-inertia power system via pole-zero cancellation. In all the aforementioned researches, the WTs have to operate in the deloading status and the kinetic energy stored in the turbine has to be harvested for frequency support. Nevertheless, the kinetic energy (KE) stored in the WT rotors is limited. Thus, WFs can only provide frequency support when the wind speed is large enough or there are enough energy reserves. Moreover, these control strategies may bring about side effects caused by the complex coupling between the WT rotors and the power system, especially frequency oscillation issues. Another drawback of the traditional approach is that WTs cannot provide long time frequency support service and their rotor speeds have to be resumed to the normal status, which may trigger a secondary frequency drop. For example, in the field experiment of [11], the WT can only provide 20.7s of frequency support as its rotor speed is about to pass the lower bound, but the grid frequency has dropped for over 33s. In the rotor speed restoration stage, the WT's electromagnetic power drops from 48.7% to 15.8% of its rated value, triggering a secondary frequency drop of 0.9Hz. From this perspective, WTs in some cases may even cause negative effects on the system frequency response dynamics.

To solve these issues, energy storage system (ESS) has been applied in WFs to improve the overall output power quality and provide ancillary services like frequency support. ESSs like battery or flywheel can both serve as energy buffers to absorb the extra wind power but also act as the energy backup system to provide extra power to bridge the gap between the demand and the supply side [16]. Meanwhile, ESS can help to smooth the wind power output and improve the system safety. For example, in [17], the authors proposed a novel control approach to smooth the wind power output with lowest ESS capacities by removing the short-period components of WF output; in [18], ESS is utilized to minimize the variations of thrust forces and shaft torques of WTs caused by fatigue loads, such that the power command from system operator can be better tracked. Due to the high flexibility and fast response of ESS, it is being implemented for system frequency support. For example, in [19], ESS is utilized to provide short term frequency support of an isolated power system; in [20], ESS is utilized to reduce the impact of wind and solar energy on the system frequency; in [21], battery type ESS is utilized to provide grid initial response. Due to the limited capacity of a single ESS, in practical situations, a group of ESSs are needed to collectively provide frequency support service, which leads to the issue of ESS cooperation, state-of-charge (SoC) monitoring and energy management. Thus, several control approaches are proposed to achieve distributed control of the ESSs. In [22], a fuzzy logic controller is proposed to achieve distributed control of the ESSs while providing enhanced frequency response, where the SoCs of the ESSs can be monitored and maintained to the desired value; in [23], a consensus approach is proposed to achieve distributed control of ESSs to achieve power regulation in WFs; similarly, in [24], a modified consensus approach based on finite time convergence principle is applied for ESSs to provide frequency support services. Although installing multiple ESSs can improve the overall frequency support capability, it requires large investment to provide the large grid scale capacity reserve. Thus, ESSs are utilized to cooperate with the WTs such that the overall system capacity can be elevated to be large enough in frequency regulation. In [25], the authors investigated on the possibility of ESSs in DFIG WTs to provide frequency response services, and they provided the needed capacities of ESS and the coordination principles to ensure effective frequency support. To determine the optimal capacity of ESS in WF, in [26], a multi-objective planning framework for battery ESS is proposed to achieve coordinated operation of ESS and WF from the perspective of various performance metrics, including the cost, lifespan, the energy level and loss of load hour. However, it fails to incorporate the way how ESS coordinates with WTs. Thus, in [27], a coordinated operation strategy for ESS to assist WTs in frequency support is proposed, where the ESSs are utilized for energy reservation and rotor speed restoration.

Nevertheless, the aforementioned researches have neglected several key issues or show certain gaps. First of all, most of the researches only consider the coordinated operation of single WT and single ESS instead of the entire wind farm. However, the frequency regulation capability of a single WT-ESS system is limited and not reliable due to low full capacity. Hence, the frequency regulation capability of an entire WF should be fully cultivated. Secondly, for some of the researches focusing on the frequency support provided by WFs, they mostly assume that all the individual WTs are operating under identical wind speed condition and neglect the wake effect existing in real world WFs [28]. The wake effect is a phenomenon which exists in

WFs where the downstream WTs receives lower wind speed than the upstream WTs as the wind speed will gradually reduce caused by energy absorbing [29]. In wind energy dominated frequency regulation, the wake effect should not be neglected because different WTs may operate in different wind speed regions, leading to different power supply mission requirements for the individual WT. Thirdly, almost all the current researches neglected the synchronous dynamics of the WTs, especially the frequency dynamics of WTs in coupled operation. When WTs are under coupled operation with the grid via virtual inertia, its rotor speed should be maintained in certain range, otherwise the WT has to be cut off the grid to ensure the synchronized operation. Hence, under low frequency operation, the WT rotor speed has to be decelerated to convert the KE into electrical power for frequency support. If the rotor speed is lower than the allowable value prior to the recovery of the frequency, the WT has to be tripped off the grid, which leads to even greater power supply shortage as well as larger frequency dip. Thus, the synchronous dynamics of WT should be fully investigated when participating in frequency support.

With the aforementioned considerations, this paper aims to propose an optimal ESS allocation scheme in WFs to improve their frequency regulation performance. The main contributions of this paper are stated as follows:

The synchronous dynamics of DFIG-based WTs to participate in frequency regulation is investigated, where the concept of frequency support margin is proposed to shape WT's frequency regulation capability;

The WTs are clustered into groups based on the received wind speed level caused by the wake effect, which serves as the basis for assigning the ESS devices to improve each WT cluster's overall stability and the ability to provide frequency support service;

An optimal ESS allocation scheme (OEA) is developed to design the capacity and placement of ESSs installed in WFs, such that all the WTs remain maximal coherency of frequency support margin, and the impact of wake effect on the frequency support capability of individual WTs can be mitigated; different from the planning framework proposed in [26], the OEA scheme in this paper considers the technical requirement of enhancing WF's frequency support capability while maintaining synchronized operation with the grid, which is helpful for mitigating the risks of secondary frequency drop and WT's being tripped off the grid.

With the above contributions and novelties, several key advantages can be brought about to the frequency support procedure of WT. Firstly, by allocating ESSs with the needed energy capacity in the different clusters of a WF, the impact of wake effect on the frequency support capability of WTs can be mitigated; secondly, by fair and appropriate allocating of the ESS in the WF, the WTs can maintain the maximal coherency in frequency support margin, such that the risk of local WTs being tripped off the grid can be minimized; thirdly, with the extra energy source from ESS, the WT's rotor speed can recover to its rated value after the system frequency is recovered, such that the rotor speed recovery procedure will not cause any secondary frequency dip to the grid. The remainder of this paper is organized as follows: Section II provides the model of WTs in frequency support; Section III proposes the optimal WT clustering approach considering the wake effect; Section IV presents the developed OEA approach; Section V conducts the simulation studies; Section VI draws a conclusion of this paper.

II. Analytical Model of DFIG-WT Frequency Dynamics

A. WT Frequency Support

Doubly fed induction generation (DFIG) is one of the key mainstream WT topologies in all the wind energy conversion systems. Thus, in this paper, DFIG-WT will be investigated as the research object. In frequency support, WT tries to harvest the hidden KE and convert it into electrical power to meet the demand. During frequency drops, DFIG will decrease its rotor speed to inject extra power to the system to compensate for load increases. After the system frequency recovers to the nominal range, the rotor speed will be restored to the maximum power point tracking (MPPT) mode. Thus, three procedures will be involved in system frequency support, including frequency drop detection, rotor speed control and rotor speed recovery [27].

For a WT, the theoretical maximum mechanical torque from the wind is given by

$$T_m = \frac{1}{2}\rho A V_\omega^3 C_p(\lambda,\beta)/\omega_m \tag{1}$$

where ρ denotes the air density; A is the blade sweep area; V_ω is the wind speed; β is the pitch angle; λ is the tip speed ratio. The aerodynamic power coefficient C_p is expressed as

$$C_p{=}0.73\left[\left(\frac{151}{\lambda_i}\right)-0.58\beta-0.02\beta^{2.14}-13.2\right]e^{(-18.4/\lambda_i)}\lambda \tag{2}$$

where $1/\lambda_i{=}(1/(\lambda-0.02\beta))-(0.003/(\beta^3+1))$.

The mechanical torque is given by

$$T_m - T_e = 2H\frac{d\omega_m}{dt} \tag{3}$$

where $T_m$is the mechanical torque from the wind; $T_e$is the electromagnetic torque; $\omega_m$is the rotor speed; $H$is the inertial constant. Meanwhile, we have the following equality

$$P_m - P_e = J\omega_m\frac{d\omega_m}{dt} \tag{4}$$

where P_m is the mechanical power from wind energy; $P_e$is the electromagnetic power; $J$is the inertia momentum. From Eq. (4), it can be seen that the additional power can be obtained by decreasing the rotor speed, and the addition power is

$$P_{WF} = -J\omega_m\frac{d\omega_m}{dt} \tag{5}$$

Thus,

$$\int_0^t \omega_m\frac{d\omega_m}{dt}dt = -\frac{P_{WF}}{J}\int_0^t dt = \frac{1}{2}\left(\omega_m^2(t)-\omega_m^2(0)\right) \tag{6}$$

$$\omega_m(t) = \sqrt{\omega_m^2(0) - 2\times\frac{P_{WF}}{J}\times t} \tag{7}$$

where $\omega_m(0)$is the initial rotor speed of the WT. It can be seen that the rotor speed is a function of the needed wind power for

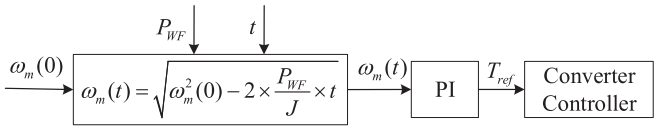

Fig. 1. Structure of the rotor speed controller.

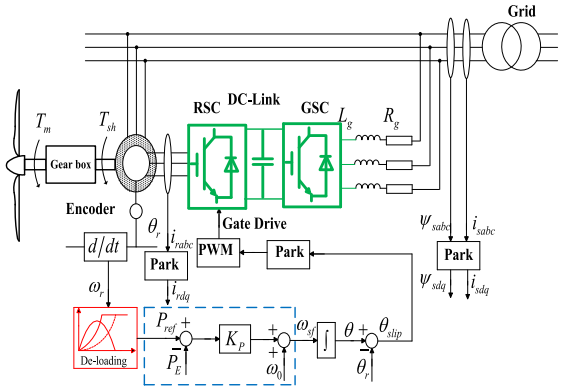

Fig. 2. P-f droop scheme of DFIG-WT.

frequency support. Hence, an extra control loop can be applied to regulate the WT rotor speed for frequency regulation, as depicted in Fig. 1.

B. WT Synchronous Dynamics

When a DFIG-WT is coupled to the main grid frequency, it is generally applied with the synchronous control to provide the voltage and frequency support capability. Thus, the P-f droop control is implemented to couple WT power output and the frequency, as depicted in Fig. 2 [30]. From Fig. 2, the P-f droop scheme is given by

$$\omega_{sf}-\omega_0=K_p(P_{ref}-P_e) \tag{8}$$

where $\omega_{sf}$is the output of the P-f droop scheme; $\omega_0$is the reference rotor speed; $K_p$is the P-f droop coefficient; P_{ref} is the reference active power given by the de-loading curve and it is a function of ω_r, as given by

$$P_{ref}{=}f_{DL}(\omega_r)=K_{DL}\omega_r^3 \tag{9}$$

where K_{DL}denotes the de-loading coefficient.

In synchronous operation, the main grid frequency are required to remain in certain range; otherwise the WT and the main grid will loss synchronization and it will not be able to provide frequency support.

For a grid-connected DFIG-WT, the swing equation of the rotor is

$$\frac{d\omega_r}{dt}=\frac{1}{T_a}\left(\frac{P_M}{\omega_r}-\frac{P_E}{\omega_r}-D\omega_r\right) \tag{10}$$

where T_a denotes the mechanical time constant; P_M is the mechanical power. Now we substitute $\omega_r$in Eq. (10) with ω_r^2,

$$\frac{d\omega_r^2}{dt}=\frac{2}{T_a}\left(P_M-P_E-D\omega_r^2\right). \tag{11}$$

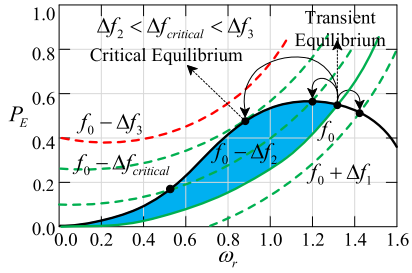

Fig. 3. WT transient equilibrium.

Meanwhile, the power angle dynamics of WT is [30]

$$\frac{d\delta}{dt}=(\omega_{sf}-\omega_g)\times 2\pi f_0, \tag{12}$$

where $\delta$is the rotor angle; $\omega_g$is the equivalent grid angular frequency. Meanwhile, the optimal mechanical power of WTs is given by [31]

$$P_M=K_W\omega_r^3 \tag{13}$$

where $K_W$is the optimal energy conversion coefficient induced by MPPT operation of the WT, and it will grow as the wind speed becomes larger.

Substituting Eq. (8)-(9), (13) into Eq. (11), (12), and replace $\delta/(2\pi f_0)$ by δ', we have the synchronous characteristics

$$\frac{d\delta'}{dt}=K_p\left(K_{DL}\omega_r^3-P_E\right)+\omega_0-\omega_g \tag{14}$$

$$\frac{d\omega_r^2}{dt}=\frac{2}{T_a}\left(K_W\omega_r^3-P_E-D\omega_r^2\right). \tag{15}$$

In Eq. (14) and (15), the rotor angle dynamics and the power angle are coupled.

C. Frequency Support Margin

Letting the right hand side of Eq. (14) and Eq. (15) equal to zero, we can obtain the synchronization characteristics of the rotor speed and the electromagnetic power, as depicted in Fig. 3. In Fig. 3, the black line denotes the solution for $d\omega_r^2/dt=0$; the other lines denote the solution for $d\delta'/dt=0$ when the grid frequency ω_g varies. Among them, the solid blue line denotes the situation when the grid frequency is the nominal value f_0. The larger intersection points of Eq. (14) and Eq. (15) are the transient equilibrium of the WT. It can be seen from Fig. 3 that, if the main grid frequency increases, say, for Δf_1 , there still will be intersection points, which indicates that the WT can maintain synchronized operation under main grid frequency rises; if the frequency drops, however, the overlapping area of the two curves will decrease and a critical frequency drop $\Delta f_{critical}$ exist when there is only one intersection point. As the frequency drop grows larger than $\Delta f_{critical}$, there will be no intersection point. Thus, $\Delta f_{critical}$is the largest frequency drop level for the WT to maintain synchronized operation.

In order to evaluate the WT's frequency support capability, we define the overlapping area of the synchronous characteristic curves in Fig. 3 as the frequency support margin (FSM). The proposed FSM can straight forwardly reflect the WT's ability to

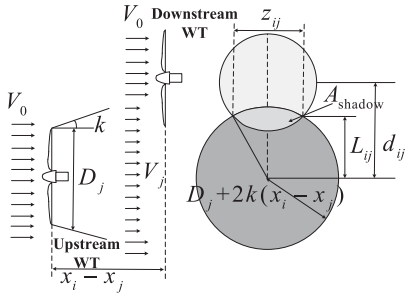

Fig. 4. Jensen's wake model.

maintain synchronized operation for frequency support under the P-f droop scheme: if $FSM \geq 0$, there will be transient equilibrium and the WT can maintain synchronized operation; if $FSM < 0$, there will be no transient equilibrium and the WT's rotor speed will keep decreasing until it is tripped from the grid. With simple calculation, the FSM has the following form:

$$FSM = \left(\frac{(K_W - K_{DL})}{4}\omega_r^4 - \frac{D}{3}\omega_r^3 + \frac{\omega_g - \omega_0}{K_p}\omega_r \right) \Bigg|_{\omega_1}^{\omega_2} \tag{16}$$

where $\omega_1 = 2\sqrt{\Phi}\cos(\frac{\theta}{3} - \frac{2\pi}{3})$, $\omega_2 = 2\sqrt{\Phi}\cos(\frac{\theta}{3})$, $\Phi = \frac{D}{3(K_W - K_{DL})}$, $\theta = \arccos(\frac{(\omega_0 - \omega_g)}{2K_p}\sqrt{\frac{27(K_W - K_{DL})}{D^3}})$.

III. WT Clustering Considering Wake Effect

A. Wake Effect Model

As the WT absorbs the energy from the wind, there will be a wake behind the turbine. In a WF, the layout of the WTs and the operation status of each WT will decide the wake effect. To investigate on the impact of wake effect on the production of power of WTs, several classic models are developed, of which the most commonly utilized one is the Jensen's model, and it will be utilized in this paper. The Jensen's model assumes that the wake expands linearly downstream the direction of the wind, as depicted in Fig. 4. The received wind speed of the ithWT is

$$v_i = v_0(1 - \delta v_i) \tag{17}$$

where $v_0$is the free wind speed; $\delta v_i$is the aggregated speed deficit. It needs to note that the received wind speed at the ithWT is affected by not only the upstream WT that is directly in front of ithWT in the wind speed direction, but also other upstream WTs that have certain degrees deviated from the wind speed direction. Thus, the aggregated speed deficit of the ith WT can be described by

$$\delta V_i = \sqrt{\sum\nolimits_{j \in N: x_j < x_i} (\delta V_{ij})^2} \tag{18}$$

$$\delta V_{ij} = \left(1 - \sqrt{1 - C_{T_j}}\right) \left(\frac{D_j}{D_j + 2k\,(x_i - x_j)} \right)^2 \left(\frac{A_{j\to i}^{shadow}}{A_i} \right) \tag{19}$$

where $D_j$is the blade diameter; $C_{T_j}$is the thrust coefficient of the turbine which represents the nonlinear relationship between the TSR and the pitch angle and can be found via a look-up table or curve fitting; $x_i - x_j$ is the distance between the upstream WT $j$and the downstream turbine $i$along the direction of the wind; $k$is the roughness coefficient and it utilizes the default value of 0.075 in this paper; $A_{j\to i}^{shadow}$is the overlapping area between the spanned wake shadow cone of WT j and the swept area of WT i , and it is calculated by

$$A_{j\to i}^{shadow} = (D_i + 2k\,(x_i - x_j))^2 \cos^{-1}\left(\frac{L_{ij}}{D_i + 2k\,(x_i - x_j)} \right) + D_i^2 \cos^{-1}\left(\frac{d_{ij} - L_{ij}}{D_i + 2k\,(x_i - x_j)} \right) - d_{ij} z_{ij} \tag{20}$$

where d_{ij}denotes the distance between the downstream WT center and the wake effect center, as shown in Fig. 4; $L_{ij}$is the distance between the wake effect center and the shadow area.

Algorithm 1: Clustering the WTs based on the received wind speed.

Input: Calculated sample data $\boldsymbol{V}^{80\times 4}$, k , maximum iteration time N.
Output: Clustering method $C = \{C_1, C_2, \ldots, C_k\}$.

```
C_t = ∅, t = 1, 2, ..., k
Select k samples from set V as the initial centroid {μ_1, μ_2, ..., μ_k}
for n ≤ N
    for i ≤ 80
        for j ≤ k
            Calculate the distance between V_i and μ_j as d_ij = ||V_i − μ_k||^2
        end for
        if d_iλ = min{d_ij}_{j=1,...,k} then C_λ = C_λ ∪ {V_i}.
        end if
        Update the centroid μ_λ.
    end for
    If μ_λ remain unchanged, then turn to (8)
    end if
end for
```

B. Impact of Wake Effect on FSM

When considering the wake effect, it is apparent that WTs in the downstream wind direction will receive lower wind speed than the upstream ones. Hence, the wake effect will also have impact on the calculated FSM shown in Eq. (16). As the wind speed increases, the optimal energy conversion coefficient K_W will increase to harvest more wind energy. The solution curve of Eq. (15) will be elevated to a higher position, as depicted by the black curves in Fig. 5. Hence, the overlapping area or the FSM, will also become larger. Reversely, if the wind speed decreases, K_W will also decrease and the FSM will become smaller. Thus, the wake effect will to some extent reduce the FSM of the WTs on the downstream wind direction. Moreover, as the wind speed decreases, the de-loading coefficient will slightly increase in order to maintain relatively larger power output for the load, which further reduces the kinetic energy reserve for frequency

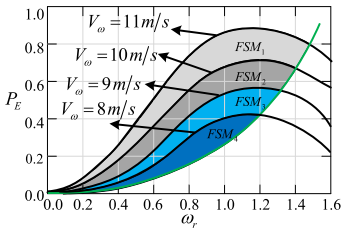

Fig. 5. Impact of wind speed on the FSM.

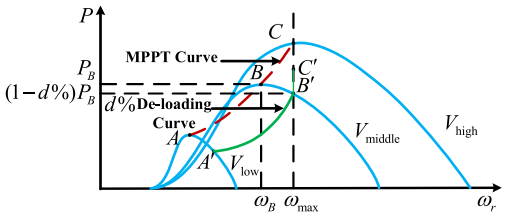

Fig. 6. WT de-loading curves under low, middle and high wind speed.

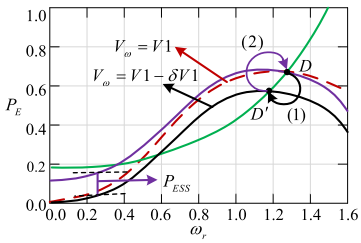

Fig. 7 Analysis of the role of ESS in synchronous characteristics.

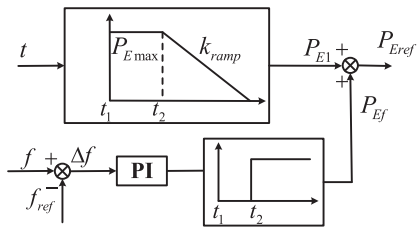

Fig. 8. Control structure for generating the reference value of ESS's power.

support. The de-loading curve of a DFIG-WT is shown in Fig. 6. In the $P_E - \omega_r$ plan, the green curve will be elevated slighted as the wind speed decreases, which further reduces the overlapping area and the FSM level.

C. Role Analysis of ESS in WT Frequency Support

Based on the previous analysis, it can be seen that engaging WTs in system frequency support can induce two kinds of risks: (1) under major system frequency drops, WTs cannot maintain synchronized operation, otherwise the rotor speed will decrease significantly, leading to tripping of the WTs; (2) under low wind speed condition, the available wind energy is limited as there are lower bounds of the rotor speed, thus, the power imbalance in frequency recovery stage and the wind energy deficiency in the rotor speed recovery stage will further increase the power gap between the supply and demand side. Out of this consideration, ESSs can largely improve the stability and reliability of WTs in frequency support.

Assume that each WT is allocated with the ESS of capacity $P_{ESS}$for both rotor speed recovery and frequency support, then it is equivalent to adding $P_{ESS}$to the mechanical power of the WT in Eq. (10). Thus, the dynamics of the rotor speed in Eq. (15) can be reconstructed as

$$\frac{d\omega_r^2}{dt} = \frac{2}{T_a}\left(K_W\omega_r^3 + P_{ESS} - P_E - D\omega_r^2\right). \tag{21}$$

Correspondingly, under a frequency drop situation, the black curves in Fig. 3 will be removed upward, as shown in Fig. 7.

In Fig. 7, due to the wake effect, the WTs in the downstream wind direction will receive the reduced wind speed $V1 - \delta V1$, and the transient equilibrium will be removed from D to D', resulting in lower rotor speed and smaller FSM. When the extra energy of P_{ESS} is added to the dynamics of rotor speed in Eq. (10), the black curves in Fig. 7 will be elevated directly to the purple curve. If the value of $P_{ESS}$is appropriate, the transient equilibrium can be recovered from D' to D again. Thus, it can be concluded that the inclusion of ESSs in frequency support is beneficial for improving the stability and reliability of WTs. It needs to note that in Fig. 7 and Fig. 7, it is difficult to calculate the critical frequency drop $\Delta f_{critical}$. Moreover, two independent WTs may have different $\Delta f_{critical}$even if they have the identical transient equilibrium. Thus, it is still more appropriate to utilize the overlapping area to shape the FSM. In Fig. 7, the calculated FSM with P_{ESS} is given by

$$FSM = \left(\frac{(K_W - K_{DL})}{4}\omega_r^4 - \frac{D}{3}\omega_r^3 + \left(\frac{\omega_g - \omega_0}{K_p} + P_{ESS}\right)\omega_r\right)\Bigg|_{\omega_1}^{\omega_2} \tag{22}$$

where ω_1, ω_2 and Φhas the same form as those of Eq. (16), except that $\theta = \arccos(\frac{(\omega_0 - \omega_g + K_P P_{ESS})}{2K_p}\sqrt{\frac{27(K_W - K_{DL})}{D^3}})$.

With respect to the control of the ESS devices, it mainly serves two purposes: to recover or maintain the rotor speed of the WTs in under-frequency scenarios, and support the system frequency when the WT is tripped off the grid or not able to provide extra power [27]. The latter mission is easier to achieve as it only requires the ESS to release its full power; while the former one is more challenging. In this paper, the rotor speed restoration scheme provided by ESS is shown in Fig. 8. In the control scheme, P_{Eref} is the final reference value for the active power output of ESS, which comprises of P_{E1} and P_{Ef}. At t_1, the WTs will start to recover its rotor speed with the help of ESS. Hence, ESS will provide its maximum power to support the WTs. At $t_2$when the system frequency has recovered to the rated value for the first time, ESS will reduce its power output with the rate of k_{ramp} to avoid overpower event. In the meantime, to reduce the impact on the frequency when the frequency is recovered for the first time, extra power from the ESS should be provided relative to the frequency deviation. Thus, extra power P_{Ef} should be added in the reference value of ESS.

TABLE I
ESTIMATED CAPACITY AND THE PERFORMANCE METRICS OF THREE CASES

Case	ESS Power Size [MW]	Frequency nadir [Hz]	Steady state frequency [Hz]
IR	44.13	49.32	49.46
PFR	98.5	49.33	49.78
IR+PFR	98.5	49.40	49.78

It needs to note that although ESSs can directly provide frequency support to the main grid, it is costly for prior stage investment and regular maintenance to utilize ESSs alone for frequency regulation in a medium or large sized power grid. In a medium or large sized power grid, the frequency regulation mission requires the output of tens to hundreds MW of active power for safety consideration [38], [39], which requires high amount of prior stage investment if ESSs alone are required to provide frequency regulation [40], [41]. For a medium sized grid with the rated active power of 1475MW, if ESSs alone are supposed to provide frequency regulation (PFR) or inertial response (IR), the needed capacity for the ESSs is estimated as shown in Table I [38]. The cost and the key technical metrics of the mainstream ESSs are given in Table II [41]. To provide sufficient power supply to meet the grid frequency regulation codes in such a medium sized grid, 145.82MW of ESS power capacity would be appropriately. It needs to note that flywheel ESSs and Lithium-ion battery ESS are more suitable for short term primary frequency control and long term frequency regulation, respectively [41]–[43]. Thus, with the needed power capacity, the minimum investment is $21.87m and $174.98m for the two type ESSs, which is high and not cost-effective.

Moreover, when the ESSs are installed to assist WTs in frequency support, it will only be utilized when the WTs are not able to recover to the original operation status under the current wind speed, or the stored energy is not sufficient to cover the power gap. Thus, a fully charged ESS can be utilized for several rounds of frequency support in ESS+WT system. However, when the ESSs are implemented for frequency regulation alone, it is more possibly that the energy will be drained off in one time frequency support, leading to the issue of battery degradation in the long term run.

Based on the previous analysis, installing ESSs in WFs to improve their frequency regulation performance is a more practical and sustainable approach than implementing ESSs alone as frequency responsive devices. In the Case Studies of this paper, it will be shown that adding ESSs in WTs can bring major improvements in its frequency support performance. Moreover, it will be shown that the ESS+WT system is more economically practical and sustainable for massively installing ESS devices for frequency regulation purposes.

IV. OPTIMAL ESS ALLOCATION IN WF

A. WT Clustering

In DFIG-WT based WFs, the collective effect of individual WTs for frequency support should be proportional to the system load level, such that the WFs have sufficient energy reserve to address sudden major load increases. As analyzed previously, ESSs can to some extent improve the individual WT's FSM. Nevertheless, due to the high investment of ESS devices, it is impossible to equip every WT with an ESS equipment. Instead, several WTs should be clustered into a group to share the ESS equipment. Consider a WF with the layout as shown in Fig. 9, where the wind speed direction is within $(0°, 90°)$. There are eight rows of ten turbines with the same rated power capacity in a parallelogram layout with a tilt degree of $7.2°$. The distance between each row and column is approximately six turbine diameters. In WT clustering, the main clustering basis is the received wind speed. In this research, WT clustering is much simpler than other conventional clustering problems. Thus, the classic K-means clustering approach is utilized in this paper.

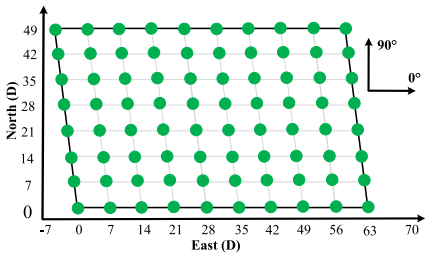

Fig. 9. Layout of the researched WF.

Firstly we calculate the received wind speed with Eq. (18), (19) and (20) when the direction of wind is $0°$, $30°$, $60°$ and $90°$, respectively. The wind speed of each WT at four angles are denoted by $\boldsymbol{V}^{80\times4}=\{\boldsymbol{V}_1, \boldsymbol{V}_2, \ldots \boldsymbol{V}_{80}\}$. Then, determine the number of clusters based on the needed energy reserves, as given by

$$k = \frac{80 \cdot P^*_{WT} \cdot \mu}{C_{ESS}} \tag{23}$$

where P^*_{WT} is the rated power of per WT, $\mu \in (0.1, 0.3)$ is the energy reservation coefficient, C_{ESS} is the rated capacity of per ESS device. After the number of clusters is determined, the clustering problem can be presented as follows

$$\min \qquad E = \sum_{l=1}^{k} \sum_{i \in C_l} |\boldsymbol{V}_i - \boldsymbol{\mu}_l|^2 \tag{24}$$

where C_l denotes the lth cluster, $\boldsymbol{\mu}_l$is called the centroid of cluster $i$in the jthwind direction, and it is given by

$$\boldsymbol{\mu}_l = \frac{1}{|C_l|} \sum_{i \in C_l} \boldsymbol{V}_i \tag{25}$$

Solving the aforementioned problem is a N-P hard problem, but it can be resolved via heuristic iteration. The solution is given in Algorithm 1.

B. Proposed Optimal ESS Allocation Scheme

In WT based power system frequency support, it is required that all the WTs in the WF can contribute to the frequency regulation mission simultaneously. Thus, it is not expected that some WTs are tripped from the mission caused by low wind

TABLE II
COMPARISON OF THE POWER, ENERGY AND COST OF THE MAINSTREAM HIGH POWER STORAGE TECHNOLOGIES

Storage technology	Energy density (Wh/kg)	Energy density (kWh/m^3)	Power density (W/kg)	Power density (MW/m^3)	Energy capital cost [m$/MWh]	Power capital cost [m$/MW]
Supercapacitor	0.5-5	4-10	1,000-10,000	0.4-10	0.5-15	0.1-0.4
SMES	1-10	0.2-2.5	500-2,000	1-4	1-10	0.2-0.5
Flywheel	10-50	20-100	500-4,000	1-2.5	2-5	0.15-0.4
Li-ion	70-200	200-600	150-500	0.4-2	0.6-2.5	1.2-4

and high frequency drop. In another word, the WTs should maintain high level of coherency in their frequency support capability. In this paper, we developed the concept of FSM to evaluate the frequency support capability of WTs. Due to the wake effect, the WTs in different location of the WF will receive different wind speed, leading to different FSM level. Nevertheless, as has been analyzed previously, the ESS devices will improve the FSM of WTs. Thus, installing ESS devices can help to alleviate the impact of wake effect on the WTs' frequency support ability. In this research, we aim to propose an optimal ESS allocation (OEA) scheme such that the WTs in a WF can maintain highest level of coherency in FSM. The proposed OEA scheme is formulated as follows:

$$\min\ I_{\text{Coherency}} = \int_{t_1}^{t_2} \sum_{i,j=1}^{n} \left(FSM_i - FSM_j\right)^2 dt \tag{26a}$$

$$\text{subject to}\, \varphi \cdot \sum_{i=1}^{n} P_{ESS,i} \le \mathcal{I} \tag{26b}$$

$$FSM_i(t) > 0, t \in (t_1, t_2), i = 1, 2, \ldots, n \tag{26c}$$

$$\omega_{\min} \le \omega_{r,i} \le \omega_{\max}, i = 1, 2, \ldots, n \tag{26d}$$

$$SOC_{\min} \le SOC^t_{ESS,i} \le 1, i = 1, 2, \ldots, n, t \in (t_1, t_2) \tag{26e}$$

$$\sum_{i=1}^{n} P_{ESS,i} \cdot SOC^t_{ESS,i} \ge \Lambda\left(\Delta f\right) - \sum_{i=1}^{n} P^t_{ref,i} \tag{26f}$$

$$\sum_{i=1}^{n} P_{ESS,i} \ge \Lambda\left(\Delta f_{critical}\right) - \sum_{i=1}^{n} P^{\min}_{ref,i} \tag{26g}$$

$$P_{ESS,\min} \le P_{ESS,i} \le P_{ESS,\max} \tag{26h}$$

$$\omega_{drop} \le \min\left\{\omega_{critical\_i}\right\}_{i=1,\cdots,n} \tag{26i}$$

where t_1 and $t_2$are the starting and ending time of frequency support, respectively; φ is the average investment for installing per unit (MW) ESS device;$\mathcal{I}$ is the total budget; $SOC^t_{ESS,i}$ and $SOC_{\min}$ are the state of charge (SOC) of the ithESS at time t and the minimum SOC level, respectively; $\omega_{\min}$, $\omega_{\max}$ are the lower and upper bound of the rotor speed, respectively; $\Lambda(\Delta f)$ is the load change that leads to frequency deviation Δf; ω_{drop} is the rotor speed reduction; $\omega_{critical\_i}$ is the critical rotor speed reduction of the ithWT.

In Eq. (26a-i), (26b) is the budget constraint, (26c) induces the lower bound of ESS capacity such that there will be transient equilibrium; (26d) and (26i) ensure that the rotor speed remains in the allowable range; (26e) denotes the bound for the SOC of the ESSs; (26f-g) indicates that the ESS's should not only serve to mitigate the impact of wake effect, but also provide energy for the grid when the wind energy is not sufficient; (26h) is the constraint for the lower and upper bound of a single ESS device.

It needs to note that the optimization problem in Eq. (26a-i) is formulated for a single WT. As analyzed previously, in reality, it is not economically appropriate and optimal to equip every WT with an ESS device. Instead, a few WTs in the same cluster should share the service of an ESS. Hence, the optimization problem is reformulated as

$$\min\ I_{\text{Coherency}} = \int_{t_1}^{t_2} \sum_{m,n=1}^{k} \left(\frac{1}{|C_m|} FSM_{\Sigma m} - \frac{1}{|C_n|} FSM_{\Sigma n}\right)^2 dt \tag{27a}$$

$$\text{subject to}\, \varphi \cdot \sum_{l=1}^{k} P_{ESS,l} \le \mathcal{I} \tag{27b}$$

$$FSM_{\Sigma m} = \sum_{i \in C_m} FSM_i \tag{27c}$$

$$FSM_i(t) > 0, t \in (t_1, t_2), i = 1, 2, \ldots, n \tag{27d}$$

$$\omega_{\min} \le \omega_{r,i} \le \omega_{\max}, i = 1, 2, \ldots, n \tag{27e}$$

$$P_{ESS,l} = \sum_{i \in C_l} \tilde{P}_{ESS,i} \tag{27f}$$

$$SOC_{\min} \le SOC^t_{ESS,l} \le 1, l = 1, 2, \ldots, k, t \in (t_1, t_2) \tag{27g}$$

$$\sum_{l=1}^{k} P_{ESS,l} \cdot SOC^t_{ESS,l} \ge \Lambda\left(\Delta f\right) - \sum_{i=1}^{n} P^t_{ref,i} \tag{27h}$$

$$\sum_{l=1}^{k} P_{ESS,l} \ge \Lambda\left(\Delta f_{critical}\right) - \sum_{i=1}^{n} P^{\min}_{ref,i} \tag{27i}$$

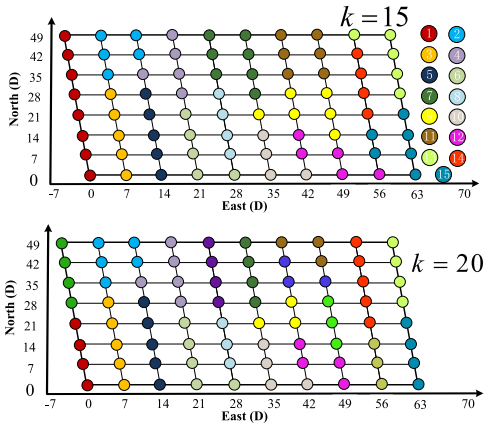

Fig. 10. WT clustering results for different cluster numbers.

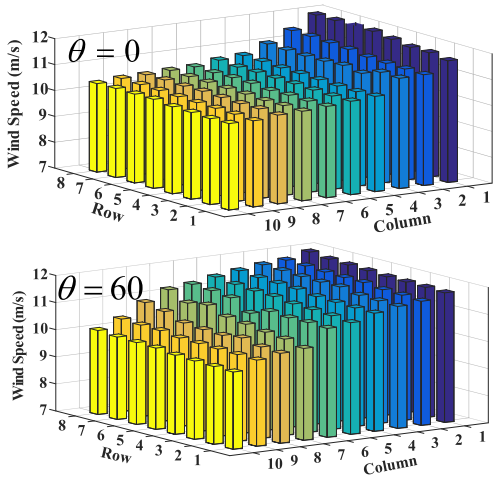

Fig. 11. Calculated wind speed profiles with different angles.

$$P_{ESS,\min} \le P_{ESS,l} \le P_{ESS,\max} \tag{27j}$$

$$\omega_{drop} \le \min\left\{\omega_{critical\_i}\right\}_{i=1,\cdots,n} \tag{27k}$$

where $FSM_{\Sigma m}$ is the total FSM of the mthcluster; $\tilde{P}_{ESS,i}$is the assigned ESS energy for the ithWT; $|C_m|$ is the number of WTs in C_m. In Eq. (27a), the optimization objective is to minimize the differences of average FSM among the WT clusters. In this problem, a WT cluster is treated as a unit. In the clustering process, the WTs with closer wind speed condition can be allocated into the same cluster. Thus, it is safe to say that high coherency among WT clusters ensures high coherency among individual WTs. In such ways, the optimization problem can be simplified to the allocation of ESS capacities for WT clusters.

V. Simulation

This section provides the simulation case studies to validate the performance of the proposed approach. Firstly, the WTs will be clustered into different groups based on the similarity of the received wind speed; secondly, the capacity of ESS device will be designed as the solution of the OEA problem (26) and (27). In the simulation, the researched WF layout is shown in Fig. 9, where the total capacity is 400MW. The range of an individual ESS's capacity is $[2MW, 5MW]$; the energy reservation coefficient is selected to be 0.12. Thus, the number of WT clusters ranges from 10 to 24. The wind speed is selected to be 12m/s from three directions, namely, 0°, 30°, 60° and 90° as shown in the reference direction frame in Fig. 9. The turbine diameters and other farm layout coefficients presented in [32]. With such settings and the developed clustering approach, the clustering result for the case when $k = 15$and $k = 20$are shown in Fig. 10. It can be seen from Fig. 10 that when the number of clusters is increased from 15 to 20, majority of the clustering results when $k = 15$ remain unchanged; instead, the new clusters are mostly originated from the original larger clusters, indicating that the clustering approach has satisfactory stability. The calculated wind speed profiles with the angle of 0° and 60°are shown in Fig. 11.

In the following cases, the number of WT cluster is selected as 15. To simplify resolving of the optimization problem, (27) is converted into a discrete problem, where the objective function is discretized as

$$I_{\text{Coherency}} = \sum_{q=1}^{n} \sum_{m,n=1}^{k} \left(\frac{1}{|C_m|} FSM_{\Sigma m} - \frac{1}{|C_n|} FSM_{\Sigma n} \right)^2 \Bigg|_{t=t_1+(q-1)\Delta t} \tag{28a}$$

where $\Delta t$is the discretization step length, $n = (t_2 - t_1)/\Delta t$. The solution set for the ESS's capacity is discretized into a finite set with the step length of 0.1 MW, i.e., $P_{ESS,l} \in \{2.0, 2.1, \ldots, 5.0\}$. In obtaining Eq. (28a), the frequency recovery curves of the grid after a load step change with only WF and the synchronous generators participating in frequency support will be obtained to determine t_1, $t_2$and the frequency nadir. Meanwhile, the Tabu Search Algorithm is utilized to solve optimization problem (27).

A. Case 1: Low Wind Speed Condition

To test the validity of the OEA scheme, a low wind speed scenario is firstly considered. In this case, the concerned wind speed is $V_{w1} = 9$m/s. The test system is given by a modified model from the 29-bus Hydro-Quebec transmission system with one DFIG WF, as shown in Fig. 12. The initial load is set as 2600MW, and a step load change of 130MW happened at $t = 5s$, which leads to the frequency drop of 0.42 Hz. With the aforementioned solutions, the optimal results for (27) are shown in Fig. 13, where the numbering of the ESSs is in accordance with Fig. 10. Correspondingly, the plots of FSMs for the WTs before and after optimization are shown in Fig. 14. In Fig. 14, the results of three scenarios are compared: without ESS, with ESS but without OEA, with both ESS and OEA. In every cluster, a WT is randomly selected to observe its FSM at the time when the system frequency reaches the nadir. It can be seen from Fig. 14(a) that when the system frequency reaches

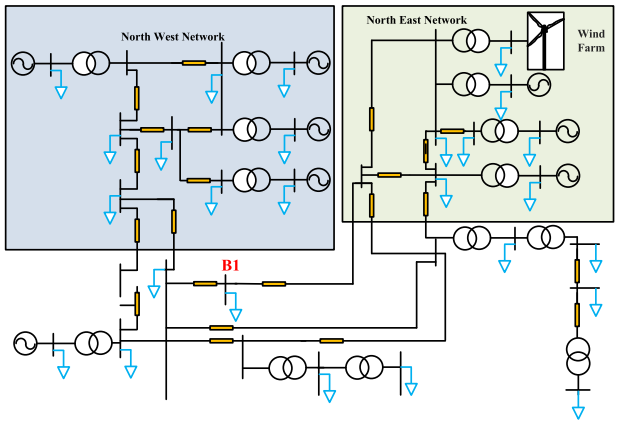

Fig. 12. Modified 29-bus test system with one DFIG-based WF.

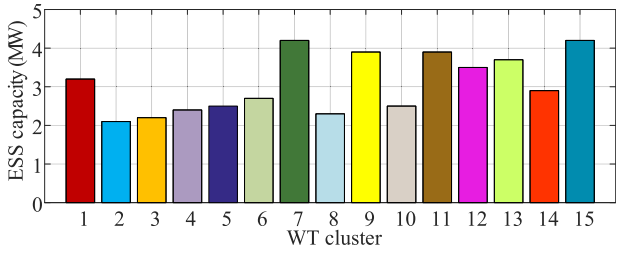

Fig. 13. Optimization results for implementing 15 ESSs in the WF.

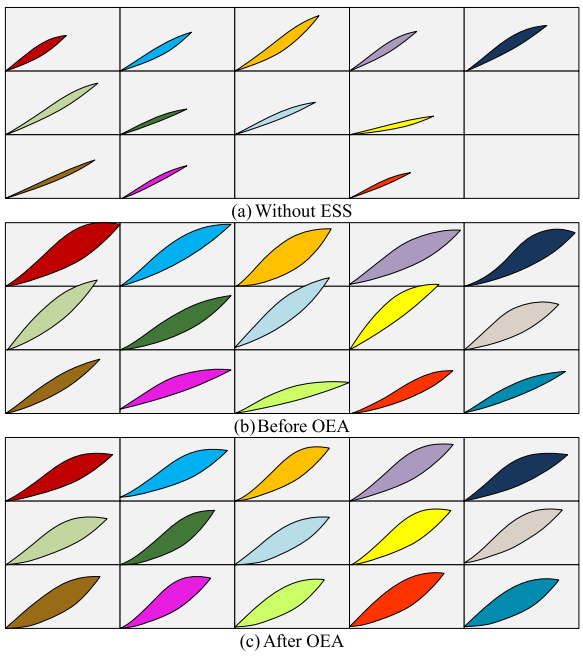

Fig. 14. Representative FSM areas from 15 clusters with three methodologies. (a) Without ESS, (b) Before OEA (c) After OEA.

the lowest level, it may have crossed the critical frequency of the WT, leading to the consequence that the WT cannot maintain synchronized operation and some WTs have to be tripped off from frequency support. By comparing Fig. 14(a) and Fig. 14(b), it can be seen that installing the ESS devices for rotor speed recovery and frequency support can significantly

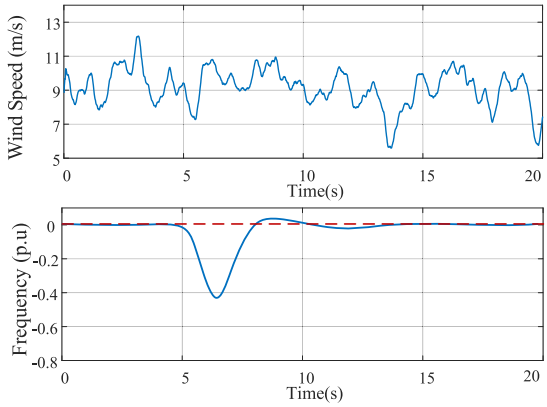

Fig. 15. Utilized variable wind speed profile and system frequency deviation.

improve the security level of WTs. Nevertheless, in Fig. 14(b), the OEA strategy was not applied; instead, the ESSs are allocated proportional to the number of WTs in each cluster to ensure that each WT is assigned with the same ESS capacity. Hence, when the wake effect is considered, the FSMs across different clusters are diversified: FSMs in the upstream wind direction are larger; FSMs in the downstream wind direction are smaller and are closer to the critical level. When the proposed OEA strategy is applied to specify the optimal ESS capacity, the FSMs across different clusters have closer area sizes, as shown in Fig. 14(c). Obviously, the impact of the wake effect on the frequency regulation performance can be effectively alleviated by installing the optimal ESS capacities.

B. Case 2: Variable Wind Speed Condition

In normal state, the wind speed is randomly changing and it can lead to power output fluctuation. Thus, it is essential to test the effectiveness of the proposed scheme under variable wind speed. The utilized wind speed profile is shown in Fig. 15. The same step load change happened at $t = 5s$ and the WTs are also engaged in frequency support. The system frequency curve is also shown in Fig. 15. Correspondingly, the representative FSM areas from 15 clusters with and without the proposed OEA are shown in Fig. 16. The selected time for plotting the FSM is $t = 7.1s$ when the frequency is near to the nadir and the wind speed is as low as 9.2m/s, such that the FSM is marginal. It can be seen from Fig. 16 that before the OEA is commenced, the FSMs of the WF is diversified. The WTs in the upper stream wind direction is relatively larger, while the FSM in the down stream wind direction is very marginal, and again there are three WTs whose FSM have reached 0. When the OEA is applied, it can be seen that the FSM level in the entire WF is equalized and it is guaranteed that every WT has FSMs larger than 0. Hence, the OEA can help to fairly distribute the energy reserve for frequency regulation.

C. Case 3: Frequency Support Performance Improvement Evaluation With ESS Support

The real performance improvement of allocating the ESSs in WF for frequency support will be validated in this case. As a

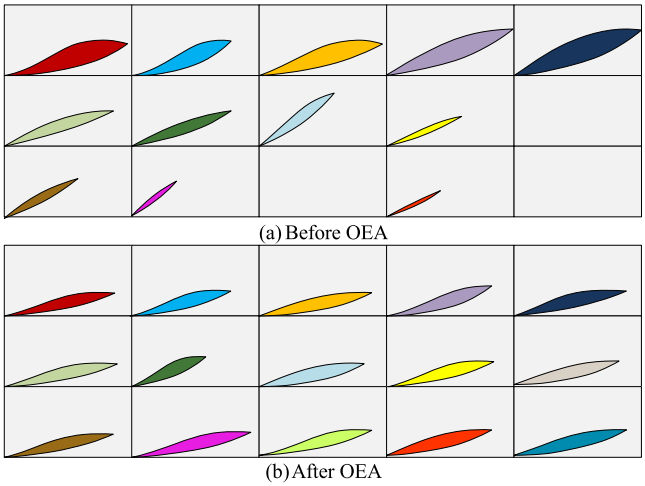

Fig. 16. Representative FSM from 15 clusters under variable wind speed. (a) Before OEA (b) After OEA.

matter of fact, ESS itself also has the capability of frequency support in the main grid. However, as has been analyzed before, it is not economically practical to install large scale ESSs for the main grid frequency support, especially in the scenarios when the main grid is large enough. Thus, in this case study, it is necessary to compare the performance of proposed DFIG-ESS frequency support scheme with the sole ESS scheme and the sole DFIG scheme, such that the practical meaning of the proposed OEA scheme can be proven. The modified 29-bus Hydro-Quebec power system shown in Fig. 12 is still utilized in the case, where the system load is set as 2600MW, and the WF has the rated capacity of 400MW. The wind speed profile is the same as the one shown in Fig. 15. In the DFIG-ESS scheme, the assigned ESSs' capacity is still given as shown in Fig. 13; in the sole ESS support scheme, to allow the ESSs directly provide frequency regulation services, 10 ESS devices are installed in the nodes of WF in Fig. 12 to replace the WTs, with each ESS having the capacity of 15MW. Under the aforementioned three frequency regulation schemes (DFIG-ESSs, DFIGs, and ESSs support), the simulation results are shown in Fig. 17, where three kinds of load step changes are assumed to test their performances.

In Fig. 17, the frequency deviations of the three methods, angular speed of DFIG with and without ESS supports, and the power output of one of the ESSs in the single ESS system and the DFIG-ESS systems are shown. It can be seen that when the load step change is 50MW and 100MW, the DFIG-ESS system shows similar performance with the ESS scheme. For the DFIG scheme which receives no support from the ESSs, the recovery time of the grid frequency and the angular speed is longer than the other schemes. This is due to the fact that ESSs have fast response for power output command. Nevertheless, when the load change is 200MW which is larger than the total capacity of the ESSs system (150MW), the ESSs cannot fully compensate for the load changes even if they are providing full capacity in power output, and the frequency nadir reaches $-0.54Hz$. For the case of the DFIG-ESS system, the load change is within its capacity range provided by the kinetic energy of the DFIG WTs in their rotational mass and the ancillary ESSs. Thus, the frequency nadir is reduced to $-0.45Hz$.

Apparently, if ESSs alone are required to provide long term frequency support, more ESSs with higher capacities are needed. In this case, approximately 240MW of ESS capacity is needed to get the same performance as that of DFIG-ESS, comparing with 46.1MW of deployed ESS in the DFIG-ESS system. Thus, when the WTs and ESSs are coordinated in frequency support, the estimated capacity requirement of ESSs can be reduced to less than 1/5 of the case when all the frequency responsive units are ESS devices. Fig. 18 shows the analysis of the prior stage investment of the Nas and the Lithium type battery ESS to fill the power gap in frequency support with ESSs alone and DFIG-ESS [26], [36], [40], [41]. It can be seen that when the DFIG-ESS system is utilized, the investment for installing the ESS devices can be reduced to 16.21% or 19.45%. From this perspective, installing ESS devices to assist the frequency support mission of WT is more economically practical than utilizing the ESSs alone.

Apart from that, it can be seen from Fig. 17 that when the ESSs alone are utilized for frequency support, they will have to provide higher power (4.85MW, 12.81MW, 15.00MW in three scenarios, respectively) to directly bridge the supply-demand gap. However, when the DFIG-ESS system is implemented, the ESSs only have to provide small portion of the capacity (1.04MW, 2.57MW, 2.83MW in three scenarios, respectively) to assist the WTs in frequency support. Moreover, the ESSs in the DFIG-ESS framework only needs to provide a shorter period of power to the grid, in contrast to the longer period with the ESSs alone (29.3s versus 43.6s, 30.6s versus 46.5s, 28.6s versus 43.7s in the scenarios, respectively). This difference will lead to the difference in ESS capacity degradation rate of the two schemes. Fig. 19 shows the capacity degradation curves of two types of battery ESSs with the aforementioned two frequency support schemes. The degradation curves are drawn by estimating the average charging/discharging times of the Nas and Lithium battery ESS in one frequency support mission when the DFIG-ESS scheme and pure ESSs scheme are adopted [19]. In Fig. 19, the abscissa is the cycle count of frequency support, and the ordinate is the capacity of the battery ESS. It shows the remained capacity of the battery ESSs when the cycle count of frequency support changes. It can be seen from Fig. 19 that when ESSs alone are required to regulate the system frequency, it will be degraded faster than those when they serve as ancillary devices of WT in frequency support, as the latter scheme will not require the ESSs to be always in the charging or discharging status during the entire frequency regulation period.

D. Case 4: Performance Comparison Under Full ESS Capacity

In order to evaluate the real performance of the proposed method, real time simulation is conducted in order to validate the effectiveness and compare the performance of the method with other traditional approaches. The modified model of the Hydro-Quebec transmission system with one DFIG WF is still

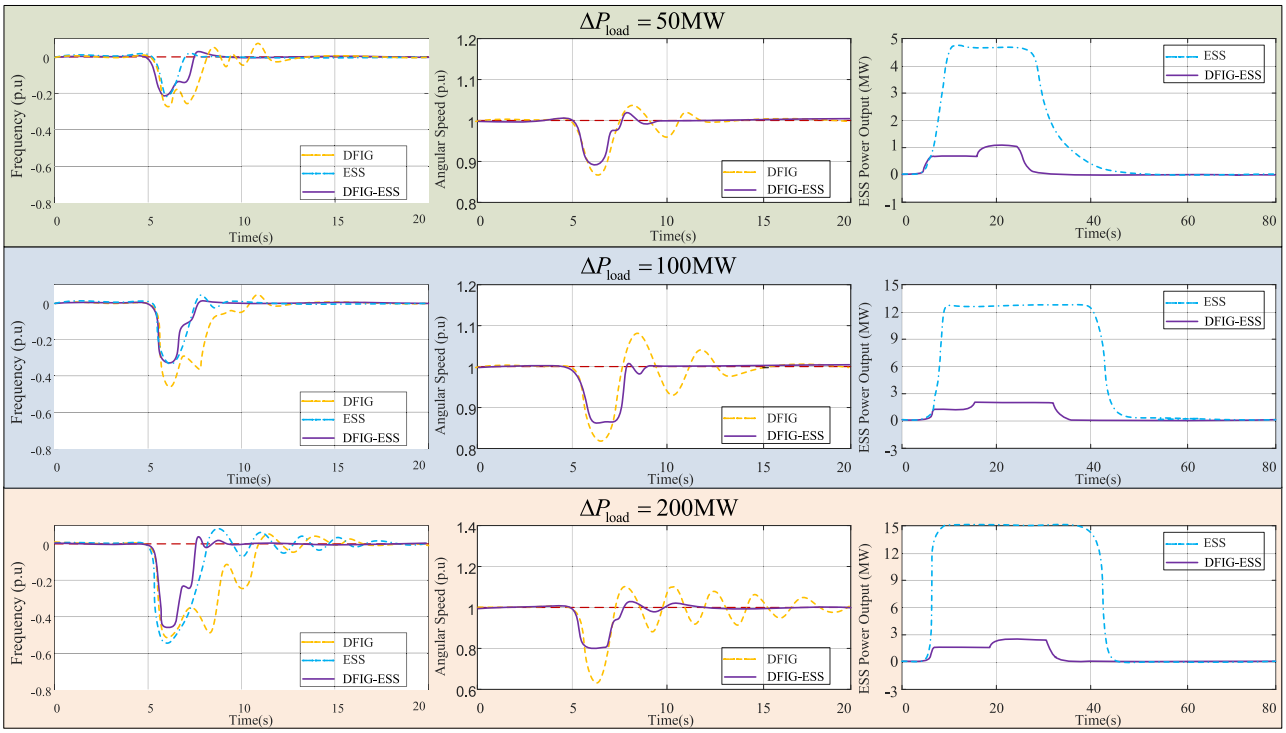

Fig. 17. Simulation results for evaluating the performance of DFIG-ESS scheme comparing with the sole ESS scheme and sole DFIG WF scheme in frequency support under three different load step changes.

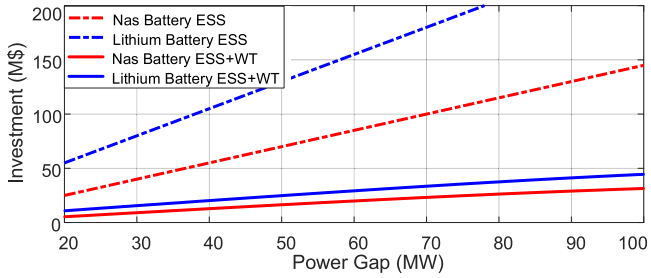

Fig. 18 Investment for installing battery ESSs to fill the grid power gap.

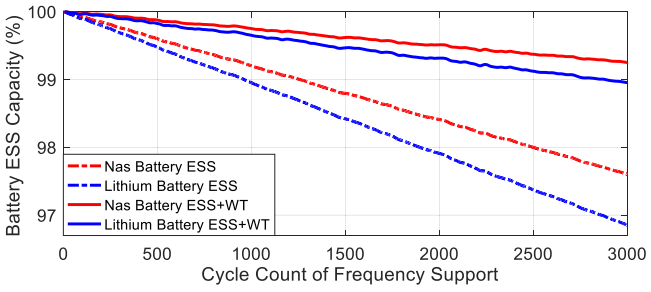

Fig. 19 Capacity degradation of battery ESS with different cycle counts.

utilized as the simulation platform, as shown in Fig. 12. The WF is rated at 400MW; the system load is 2600MW; the per unit power for ESS device is set as 5MW. In this case, the traditional frequency support scheme without ESS [33] (TFS), and the coordinated frequency support [20] under empiric allocation of ESS (CFSEA) method (proportional allocation of ESS's capacity based on the capacity of each row in the WF) are incorporated for comparison purpose. In the simulation, a load change of 150MW happened at bus B1, causing some system frequency fluctuation. It is assumed that the wind speed is fluctuating as shown in Fig. 15 with the average speed being 9.2m/s. The transient responses of the grid frequency, the WT rotor speed and the active power output of the WF and the ESS with three methods are shown in Fig. 20. In Fig. 20, (a1)-(a4) show the results of the TFS approach; (b1)-(b4) show the results of the proposed OEA approach; (c1)-(c4) show the results of CFSEA. It can be seen from (a1) that when a major load change happens, the largest frequency deviation can reach 0.57Hz. When the ESS devices are implemented, the system frequency deviation can be reduced to some extent, as shown in (c1). However, in frequency support, WTs is capable of maintaining synchronized operation only if there is equilibrium in the synchronization characteristic curves. Thus, there are 12 WTs losing their synchronization and they have to be tripped off the grid when no ESS device is implemented, as shown in (a2). In (c2), as the frequency continues to decrease, some of the WTs in the downstream wind direction may still lose their synchronization despite the assistance of the ESSs, because the assigned capacity of the ESSs in the downstream wind direction is not able to render the impact of the wake effect. As the frequency continues to drop in (c1), the ESSs have to provide secondary support by increasing their power output to recover the frequency, as shown in (c4).

When the proposed OEA approach is applied, all the WTs in each WT cluster can share closer FSM level such that there is much lower risk of some WTs losing their synchronization. Hence, in this case, all the WTs can maintain synchronized

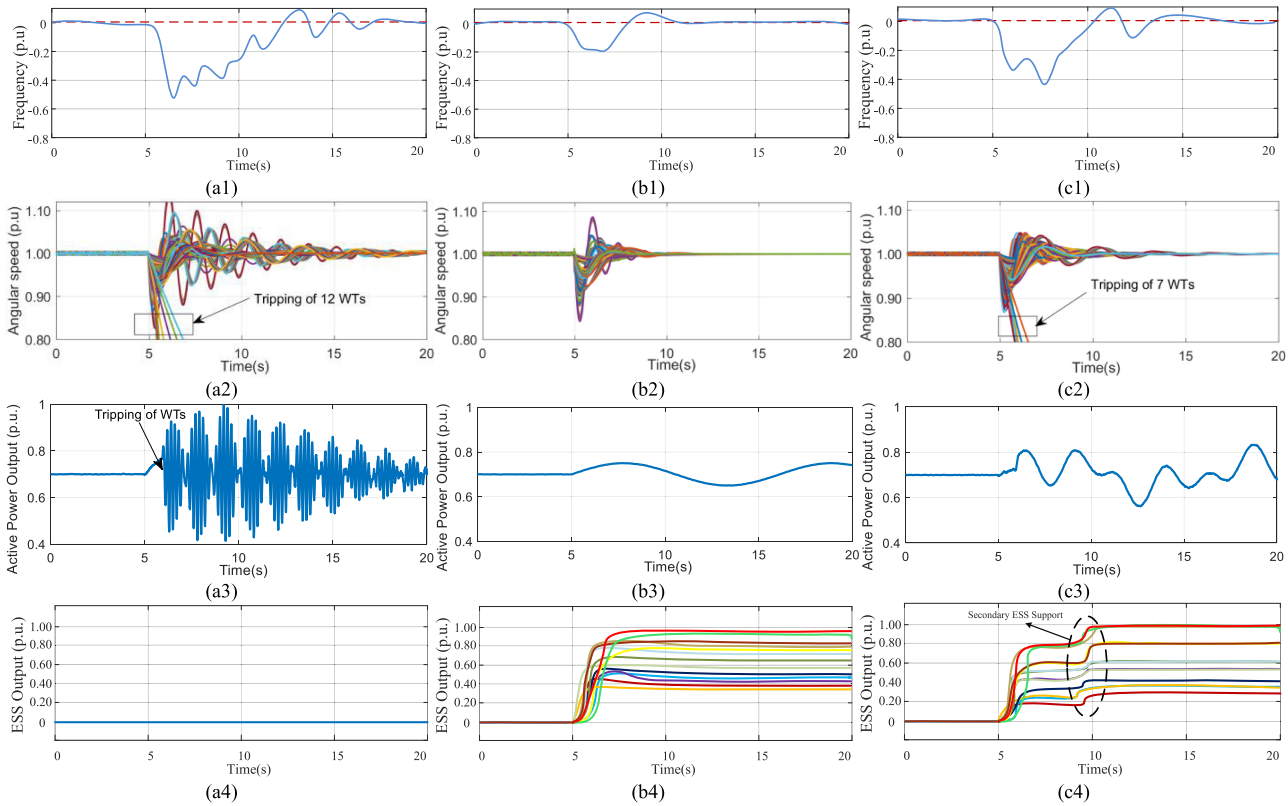

Fig. 20 Transient response of system frequency, WT rotor speed and active power output of WF and ESS: (a1)-(a4) TFS; (b1)-(b4) OEA; (c1)-(c4) CFSEA.

operation, as shown in (b2). Moreover, it can be seem from (b4) that each ESS in a cluster can contribute to different active powers for frequency control, while in (c4), some ESSs may provide equal active power as their capacities are specified based on the capacity of the WTs in the same row instead of the actual need for maintaining safety. Overall, the proposed OEA scheme shows better performance in frequency support, as can be seen from (b1) that the frequency deviation nadir is flattened by the ESSs and the frequency can recover to the normal value in a faster manner.

E. Case 5: Performance Comparison and Evaluation Under Different ESS Energy Levels and Wind Speed Condition

To show the performance of the proposed OEA scheme under different operation status, another comparative study is conducted. In this comparative study, the multi-objective planning framework (MOPF) from [19] is taken for comparison purpose. In Case 3, the performance of the OEA scheme is tested under identical ESS and wind speed condition. However, the real world scenario will be much more complicated as the wind speed varies and the ESSs' energy level may also change. Thus, it is necessary to compare the performance of the OEA scheme with MOPF under different wind speed and ESS energy levels. In this study, four scenarios are assumed and executed as the operation conditions: Scenario1—high wind speed and 100% ESS energy level; Scenario2—high wind speed and 30% ESS energy level; Scenario3—low wind speed and 100% ESS energy level; Scenario4—low wind speed and 30% ESS energy level, where low wind speed means the wind speed is lower than 9m/s. With the four scenarios, the simulation results of the two approaches are shown in Fig. 21.

In Fig. 21, each box shows the comparative results of the two methods under one of the four scenarios. In each box, the left column images show the simulation results of MOPF, while the right column images show the results of OEA. It can be observed from the frequency deviation curves that the recovery of WT speed can lead to a secondary frequency dip. Under Scenario 2 and Scenario 4 with MOPF, the secondary frequency dip might be even larger than the primary frequency dip. With the proposed OEA approach, the secondary frequency dip can be almost mitigated. In fact, the secondary frequency dip is mainly caused by two factors: the tripping of some WTs and the rotor speed recovery. It can be seen from the results of Scenario 2-4 that when the MOPF is utilized, some of the WTs will lose its synchronization with the grid and they have to be tripped off the grid, leading to a secondary frequency dip. This is caused by the fact that the ESS capacities with MOPF are not allocated to improve the FSM, such that some of the WTs may have no FSM under a major grid frequency dip and low wind speed. With the proposed OEA, however, all the WTs can maintain frequency support status under all the four scenarios. Thus, the proposed OEA approach has superior performance over MOPF in the frequency support missions.

In the above discussion, two different energy levels of ESSs are assumed to compare the performance. It can be seen that

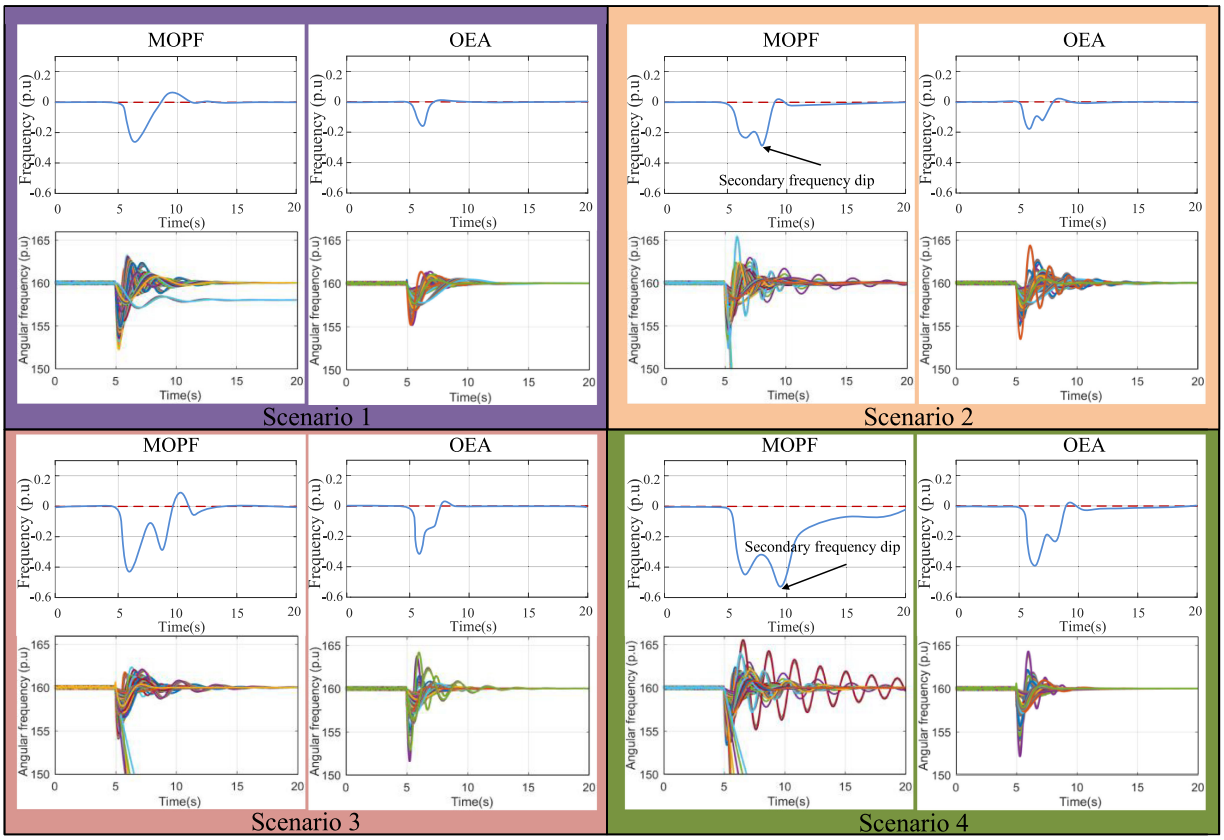

Fig. 21 Performance comparison under different ESS and wind speed conditions.

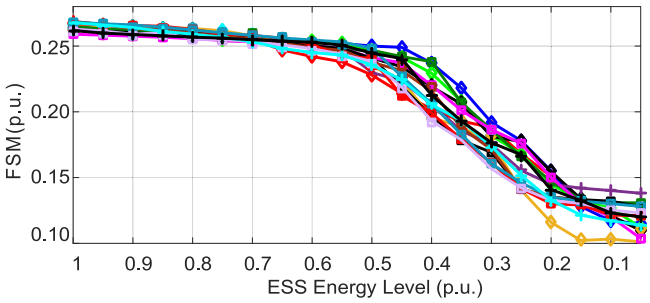

Fig. 22. Analysis of impact of ESS energy level on FSM.

the energy level of ESSs indeed has impact on the performance of the methods. Thus, it is necessary to evaluate the impact of the initial energy level of the ESSs on the overall performance, such that the needed energy levels for safeguarding the system security will be determined. In this study, we lowered down the energy level of each ESS distributed in the WF simultaneously in a stepwise manner, i.e., lowering down the initial energy level for 5% for per trial. The FSMs of the representative WTs within the 15 clusters are calculated under the same simulation condition of Case 2. The relationships between the calculated FSMs and the ESSs' energy level are shown in Fig. 22. It general, it can be seen that as the ESS's energy level decreases, the FSM of the WTs will also decrease. However, the FSM decreases are not proportional to the reduction of the ESS energy level. Instead, when the ESSs' energy levels are relatively large, e.g., larger than 50% or 60%, the FSMs will decrease slowly and all the FSMs remain high coherency. As the energy levels continue to decrease, the FSMs will reduce in a faster manner. However, the FSMs can still maintain certain degree of coherency. Until the energy provided by the ESSs is dried off, the remained FSMs are provided only by the WTs. Thus, it can be concluded from Fig. 22 that as long as the energy levels of ESS with the assigned capacity are larger than approximately 50% of the full capacity, the FSM will only endure minor impact from energy level changes and all the WTs can maintain high coherency in FSMs. Even if the energy level is lower than 50% of the rated value, the ESSs can still induce high FSM augmentation on basis of the FSM levels provided by WTs alone.

Fig. 23 shows the primary and secondary frequency nadir of the system under different wind speed condition and ESSs energy levels, where the blue curves represent the low wind speed (9m/s) condition, while the red curves represent the high wind speed condition (11.5m/s). It can be seen that when the wind speed is high, the change of the energy level only has minor impact on the system frequency nadir; when the wind speed is low, the reduction of ESS's energy level will lead to major increase of frequency nadir, suggesting that the impact of ESS energy level changes on the system performance under low wind speed is greater than that when the wind speed is high. From this perspective, the value of ESS is more prominent under low wind speed scenarios.

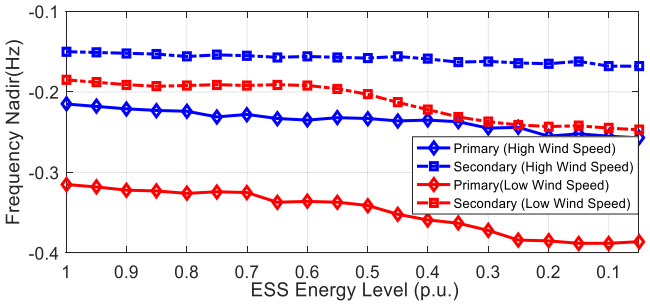

Fig. 23. Analysis of impact of ESS energy level on the frequency nadir.

VI. Conclusion

This paper proposed an optimal ESS allocation solution for WTs to engage in power system frequency support considering the impact of the wake effect. Firstly, the synchronous stability of WTs when coupled with the grid frequency is analyzed with the concept of frequency support margin, which helps to explain the mechanism why WTs can lose their synchronous stability under major grid frequency drops. In the meantime, the impact of the wake effect in WFs on individual WT's FSM in under frequency scenarios is analyzed. Subsequently, the importance of ESS's extra power for mitigating the impact of wake effect is elaborated. ESSs can both provide extra power for system frequency support and help to recover the rotor speed of WTs. Considering the received wind speed in different WTs, a WT clustering method is proposed such that the WTs within the same cluster will be sharing the same ESS. Afterwards, an OEA scheme is proposed which tries to optimize the coherency of all the WT cluster's FSM, such that all the WTs can maintain the same synchronous stability. Simulation studies are conducted to show the effectiveness of the proposed OEA. With the OEA scheme, the risk of WTs losing their synchronous stability can be reduced, and the actual performance of WFs engaging in power system frequency support can be improved. It needs to note that the main limitation of the proposed scheme is that it requires the investment for deploying the ESSs. However, as a kind of ancillary device, ESSs do not directly provide frequency support service to the grid; instead, it serves to improve the system security and WT's frequency support capability. Thus, the needed capacity of ESSs is not so large as the case when the ESSs are directly providing frequency support. In such case, the investment of deploying ESSs can be maintained to a lower level.

References

[1] P. N. Papadopoulos and J. V. Milanovic, "Probabilistic framework for transient stability assessment of power systems with high penetration of renewable generation," *IEEE Trans. Power Syst.,* vol. 32, no. 4, pp. 3078–3088, Jul. 2017.

[2] M. F. M. Arani and E. F. El-Saadany, "Implementing virtual inertia in DFIG-based wind power generation," *IEEE Trans. Power Syst.,* vol. 28, no. 2, pp. 1373–1384, Jun. 2013.

[3] K. V. Vidyanandan and N. Senroy, "Primary frequency regulation by deloaded wind turbines using variable droop," *IEEE Trans. Power Syst.*, vol. 28, no. 2, pp. 837–846, May 2013.

[4] M. E. I. Mostafam, V. Courtecuise, C. Saudemont, B. Robyns, and J. Deuse, "Fuzzy logic supervisor-based primary frequency control experiments of a variable-speed wind generator," *IEEE Trans. Power Syst.,* vol. 24, no. 1, pp. 407–417, Feb. 2009.

[5] J. Brisebois and N. Aubut, "Wind farm inertia emulation to fulfill hydro-Qu´ebec's specific need," in *Proc. IEEE Power Energy Soc. Gen. Meeting*, Detroit, MI, USA, 2011, pp. 1–7.

[6] V. Gevorgian, Y. Zhang, and E. Ela, "Investigating the impacts of wind generation participation in interconnection frequency response," *IEEE Trans. Sustain. Energy,* vol. 6, no. 3, pp. 1004–1012, Jul. 2015.

[7] M. Kayikci and J. V. Milanovic, "Dynamic contribution of DFIG-based wind plants to system frequency disturbances," *IEEE Trans. Power Syst.,* vol. 24, no. 2, pp. 859–867, May 2009.

[8] Goldwind. Findings from the demonstration of inertia based fast frequency response—A field study at Gullen Range wind farm knowledge sharing report, 2019, [Online]. Available: https://arena.gov.au/assets/2020/10/field-study-at-gullen-range-wind-farm.pdf

[9] T. Ahmad *et al.*, "Field implementation and trial of coordinated control of wind farms," *IEEE Trans. Sustain. Energy,* vol. 9, no. 3, pp. 1169–1176, Jul. 2018.

[10] R. J. Piwko, N. W. Miller, and J. M. MacDowell, "Field testing and model validation of wind plants," in *Proc. IEEE Energy Soc. Gen. Meeting*, Pittsburgh, PA, USA, Jul. 2008, pp. 1–9.

[11] Y. Cui, P. Song, X. S. Wang, W. X. Yang, H. Liu, and H. M. Liu, "Wind power virtual synchronous generator frequency regulation characteristics field test and analysis," in *Proc. 2nd Int. Conf. Green Energy Appl.*, Singapore, Mar. 2018, pp. 193–196.

[12] Y. Zhang, M. E. Raoufat, K. Tomsovic, and S. M. Djouadi, "Set theory based safety supervisory control for wind turbines to ensure adequate frequency response," *IEEE Trans. Power Syst.,* vol. 34, no. 1, pp. 680–692, Jan. 2019.

[13] S. Wang and K. Tomsovic, "Fast frequency support from wind turbine generators with auxiliary dynamic demand control," *IEEE Trans. Power Syst.*, vol. 34, no. 5, pp. 3340–3348, Sep. 2019.

[14] M. M. Kabsha and Z. H. Rather, "A new control scheme for fast frequency support from HVDC connected offshore wind farm in low inertia system," *IEEE Trans. Sustain. Energy,* vol. 11, no. 3, pp. 1829–1837, Jul. 2020.

[15] M. A. M. Manaz and C. N. Lu, "Design of resonance damper for wind energy conversion system providing frequency support service to low inertia power systems," *IEEE Trans. Power Syst.,* vol. 35, no. 6, pp. 4297–4306, Nov. 2020.

[16] L. Meng *et al.*, "Fast frequency response from energy storage systems-A review of grid standards, projects and technical issues," *IEEE Trans. Smart Grid,* vol. 11, no. 2, pp. 1566–1571, Mar. 2020.

[17] K. Koiwa, T. Ishii, K. Liu, T. Zanma, and J. Tamura, "On the reduction of the rated power of energy storage system in wind farms," *IEEE Trans. Power Syst.,* vol. 35, no. 4, pp. 2586–2595, Jul. 2020.

[18] S. Huang, Q. Wu, Y. Guo, and F. Rong, "Hierarchical active power control of DFIG-based wind farm with distributed energy storage systems based on ADMM," *IEEE Trans. Sustain. Energy,* vol. 11, no. 3, pp. 1528–1538, Jul. 2020.

[19] G. Delille, B. Francois, and G. Malarange, "Dynamic frequency control support: A virtual inertia provided by distributed energy storage to isolated power systems," in *Proc. IEEE PES ISGT Eur. Conf.*, 2010, pp. 1–8.

[20] G. Delille, B. Francois, and G. Malarange, "Dynamic frequency control support by energy storage to reduce the impact of wind and solar generation on isolated power system's inertia," *IEEE Trans. Sustain. Energy*, vol. 3, no. 4, pp. 931–939, Oct. 2012.

[21] V. Knap, R. Sinha, M. Swierczynski, D. Stroe, and S. Chaudhary, "Grid inertial response with lithium-ion battery energy storage systems," in *Proc. IEEE 23rd ISIE*, 2014, pp. 1817–1822.

[22] F. Sanchez, J. Cayenne, F. Gonzalez-Longatt, and J. L. Rueda, "Controller to enable the enhanced frequency response services from a multi-electrical energy storage system," *IET Gener. Transm. Distrib.*, vol. 13, no. 2, pp. 258–265, Jan. 2019.

[23] S. Baros and M. D. Ilic, "A consensus approach to real-time distributed control of energy storage systems in wind farms," *IEEE Trans. Smart Grid*, vol. 10, no. 1, pp. 613–625, Jan. 2019.

[24] Y. Wang *et al.*, "Aggregated energy storage for power system frequency control: A finite-time consensus approach," *IEEE Trans. Smart Grid,* vol. 10, no. 4, pp. 3675–3686, Jul. 2019.

[25] J. Kim, E. Muljadi, V. Gevorgian, and A. F. Hoke, "Dynamic capabilities of an energy storage-embedded DFIG system," *IEEE Trans. Ind. Appl.*, vol. 55, no. 4, pp. 4124–4134, Jul. 2019.

[26] S. Paul, A. P. Nath, and Z. H. Rather, "A multi-objective planning framework for coordinated generation from offshore wind farm and battery energy storage system," *IEEE Trans. Sustain. Energy,* vol. 11, no. 4, pp. 2087–2097, Oct. 2020.
[27] L. Miao, J. Wen, H. Xie, C. Yue, and W. Lee, "Coordinated control strategy of wind turbine generators and energy storage equipment for frequency support," *IEEE Trans. Ind. Appl.,* vol. 51, no. 4, pp. 2732–2742, Jul. 2015.
[28] P. Kou, D. Liang, and L. Gao, "Distributed coordination of multiple PMSGs in an islanded DC microgrid for load sharing," *IEEE Trans. Energy Convers.*, vol. 32, no. 2, pp. 471–485, Jun. 2017.
[29] X. Lyu, Y. Jia, and Z. Xu, "A novel control strategy for wind farm active power regulation considering wake interaction," *IEEE Trans. Sustain. Energy,* vol. 11, no. 2, pp. 618–628, Apr. 2020.
[30] L. Huang, H. Xin, L. Zhang, Z. Wang, K. Wu, and H. Wang, "Synchronization and frequency regulation of DFIG-based wind turbine generators with synchronized control," *IEEE Trans. Energy Convers.,* vol. 32, no. 3, pp. 1251–1262, Sep. 2017.
[31] V. Akhmatov, *Induction Generators for Wind Power.* Brentwood, U.K.: Multi-Science, 2005.
[32] K. S. Hansen, "Wake measurements used in the model evaluation," Jun. 2008. [Online] Available: http://www.upwind.eu/pdf/D8.1%20-%20Wake%20 measurements%20used%20in%20the%20model%20evaluation.pdf
[33] X. Peng, W. Yao, C. Yan, J. Wen, and S. Cheng, "Two-stage variable proportion coefficient based frequency support of grid-connected DFIG-WTs," *IEEE Trans. Power Syst.,* vol. 35, no. 2, pp. 962–974, Mar. 2020.
[34] C. K. Zhang, L. Jiang, Q. H. Wu, Y. He, and M. Wu, "Delay-dependent robust load frequency control for time delay power systems," *IEEE Trans. Power Syst.,* vol. 28, no. 3, pp. 2192–2201, Aug. 2013.
[35] D. Rerkpreedapong, A. Hasanovic, and A. Feliachi, "Robust load frequency control using genetic algorithms and linear matrix inequality," *IEEE Trans. Power Syst.,* vol. 18, no. 2, pp. 855–861, May 2003.
[36] Energy storage association, Sodium Sulfur (NaS) Batteries, 2019. [Online]. Available: http://energystorage.org/energy-storage/technologies/sodium-sulfur-nas-batteries
[37] S. Bradbury, J. Hayling, P. Papadopoulos, and N. Heyward, *Smarter Network Storage Electricity Storage in GB: SNS 4.7 Recommendations for Regulatory and Legal Framework (SDRC 9.5)*, U.K. Power Netw., London, U.K., Sep. 2015.
[38] V. Knap, S. K. Chaudhary, D. I. Stroe, M. Swierczynski, B. I. Craciun, and R. Teodorescu, "Sizing of an energy storage system for grid inertial response and primary frequency reserve," *IEEE Trans. Power Syst.,* vol. 31, no. 5, pp. 3447–3456, Sep. 2016.
[39] V. Knap, R. Sinha, M. Swierczynski, D.-I. Stroe, and S. Chaudhary, "Grid inertial response with Lithium-ion battery energy storage systems," in *Proc. IEEE 23rd Int. Symp. Ind. Electron.*, 2014, pp. 1817–1822.
[40] European Association for Storage of Energy (EASE) and European Energy Research Alliance (EERA), "European energy storage technology development roadmap towards 2030," EASE/EERA, Tech. Rep., Mar. 2013.
[41] M. Farhadi and O. Mohammed, "Energy storage technologies for high-power applications," *IEEE Trans. Ind. Appl.*, vol. 52, no. 3, pp. 1953–1961, May/Jun. 2016.
[42] F. Zhang, M. Tokombayev, Y. Song, and G. Gross, "Effective flywheel energy storage (FES) offer strategies for frequency regulation service provision," in *Proc. Power Syst. Comput. Conf.*, Aug. 2014, pp. 1–7.
[43] D. Ketata and L. Krichen, "Control and power management of a PEMFC supercapacitor as a distributed generator," in *Proc. 8th Int. Multi-Conf. Syst. Signals Devices*, Mar. 2011, pp. 1–7.

Linyun Xiong received the Ph.D. degree in electrical engineering from Shanghai Jiao Tong University, China, in 2019. He is currently with the School of Electrical Engineering, Chongqing University, Chongqing, China. His research interests include power system nonlinear control, sliding mode control, Hamiltonian system, and robust control.

Shaobo Yang received the B.S. degree from the Hebei University of Engineering. He is currently working toward the M.S. degree with Chongqing University. His research interests include power system stability, nonlinear control, and power system oscillation damping.

Sunhua Huang received the M.S. degree in electrical engineering from Hunan University, China, in 2018. He is currently working toward the Ph.D. degree in electrical engineering with the School of Electrical Information and Electronic Engineering, Shanghai Jiao Tong University. His research interests focuses on the nonlinear control of power system and renewable energy.

Donglin He received the B.S. degree from the University of South China. He is currently working toward the M.S. degree with Chongqing University. His research interests include power system reliability, wind energy integration and multi-energy system.

Penghan Li received the B.S. degree in electrical engineering from the Harbin Institute of Technology, China, in 2016. He is currently working toward the Ph.D. degree in electrical engineering with the School of Electrical Information and Electronic Engineering, Shanghai Jiao Tong University. His research interests include power system stability analysis and control.

Muhammad Waseem Khan received the Ph.D. degree from Shanghai Jiao Tong University, China, where he is currently working as a Postdoctoral Research Fellow. His research interest includes multi-agent system, power system reliability, and renewable energy.

Jie Wang received the Ph.D. degree in industrial automation from Northeast University, China, in 1998. He is a Professor of power system and its automation with the Department of Electrical Engineering of Shanghai Jiao Tong University and a laboratory for the development of Flexible AC/DC transmission system technology and intelligent control with the same University. His research interests include stability analysis and control of complex power system, smart grids, and to establish a series of theoretical analysis results of nonlinear differential algebraic control systems and apply these results to the nonlinear control of structure preserving power systems. Based on the differential algebraic Hamiltonian system and its periodic solution theory, the low frequency oscillation analysis and control method of interconnected power grid are presented. The symmetry and conserved quantity in Noether's theory are applied to restrict the existence of periodic solutions of power system.